

# Cosmic ray acceleration at oblique shocks

A. R. Bell\*, K.M. Schure and B. Reville

*Clarendon Laboratory, University of Oxford, Parks Road, Oxford OX1 3PU, UK*

## ABSTRACT

We show that the diffusion approximation breaks down for particle acceleration at oblique shocks with velocities typical of young supernova remnants. Higher order anisotropies flatten the spectral index at quasi-parallel shocks and steepen the spectral index at quasi-perpendicular shocks. We compare the theory with observed spectral indices.

**Key words:** cosmic rays, acceleration of particles, shock waves, ISM: supernova remnants

## 1 INTRODUCTION

The well-established theory of cosmic ray (CR) acceleration by strong non-relativistic shocks predicts a differential energy power law spectrum  $n(E)dE \propto E^{-s}dE$  with a spectral index  $s = 2$  (Axford, Leer & Skadron 1977, Krimskii 1977, Bell 1978, Blandford & Ostriker 1978). However, a variety of spectral indices is observed. Galactic CR have a steeper spectrum even when allowance is made for energy-dependent propagation losses (Hillas 2005). Steeper spectra are also observed in young supernova remnants (SNR) as discussed below. Deviations from a  $s = 2$  spectrum are well known for relativistic shocks (for example: Kirk & Heavens 1989, Ostrowski 1991, Baring Ellison & Jones 1993, Ruffalo 1999, Gieseler et al 1999, Kobayakawa, Honda & Samura 2002, Achterberg et al 2001). Here we show that corrections to theory produce a spectral index that deviates significantly from  $s = 2$  even at shock velocities as low as 10,000 km s<sup>-1</sup> typical of young supernova remnants. The magnitude of the effect depends on the ratio of the velocity of the accelerating particle to the shock velocity. Hence, it may also apply to the acceleration of non-relativistic particles at heliospheric shocks. The spectrum can either steepen or flatten depending on the angle between the shock normal and the large scale upstream magnetic field. Quasi-perpendicular shocks (Jokipii 1982, 1987) show particularly strong steepening. The effect is small for parallel shocks where changes in the spectral index are second order in the ratio of the particle velocity to the shock velocity. Non-linear hydrodynamic feedback of the CR pressure onto the shock structure can also change the spectral index (Drury 1983, Dury & Völk 1981, Ellison, Baring & Jones 1996) but we do not take account of this in the present paper. We assume that the fluid velocity is uniform both upstream and downstream of the shock. A further assumption lying at the heart of our

method is that the magnetic field can be divided into (i) a large scale field that is uniform apart from a change of direction and magnitude at the shock and (ii) a small scale field that fluctuates on scales smaller than the CR Larmor radius and deflects the CR trajectories through small angles to cumulatively scatter the CR. This ignores magnetic field line wandering which can also change the CR spectral index (Kirk, Duffy & Gallant 1996). In our calculations we further assume that the fluid is always compressed by a factor of four at the shock, which neglects the increase in compression at the shock due to the different equation of state of the relativistic component (ratio of specific heats = 4/3) and the effects of finite Mach number. With these assumptions we isolate and concentrate on the breakdown of the diffusive approximation and the effect of high order anisotropies in the CR distribution near the shock.

## 2 EQUATIONS

Cosmic rays are thought to be accelerated to high energy by crossing back and forth across a shock in a first order Fermi process, with a fractional energy gain of order  $u_s/c$  at each crossing where  $u_s$  is the shock velocity. A small proportion of the CR injected at low energy proceed to cross the shock many times before escaping the shock environment. Statistically this results in a power law stretching up to a few PeV in the galaxy and probably approaching ZeV extragalactically. Here we consider CR protons of mass  $m_p$ , but the analysis applies equally well to heavier ions or to electrons. The shape and extent of the CR spectrum is described by the CR distribution function  $f(x, \mathbf{p}, t)$  in momentum  $\mathbf{p}$ . We locate a planar shock at  $x = 0$ . Upstream of the shock ( $x < 0$ ) the ambient plasma flows towards the shock at the shock velocity  $u_s$ . For a strong non-relativistic shock the plasma velocity is reduced to  $u_s/4$  in the downstream plasma. The

\* E-mail: t.bell1@physics.ox.ac.uk

equation for the CR distribution function is

$$\frac{\partial f}{\partial t} + (v_x + u) \frac{\partial f}{\partial x} - \frac{\partial u}{\partial x} p_x \frac{\partial f}{\partial p_x} - \frac{u}{c} \frac{\partial u}{\partial x} p \frac{\partial f}{\partial p} + e\mathbf{v} \wedge \mathbf{B} \cdot \frac{\partial f}{\partial \mathbf{p}} = C(f) \quad (1)$$

where  $f$  is defined in the local fluid rest frame moving at velocity  $u(x)$  in the  $x$  direction and relativistic effects due to  $\gamma_u = (1 - u^2/c^2)^{-1/2} \neq 1$  have been neglected.  $v_x$  is the  $x$ -component of the CR velocity  $\mathbf{v}$ ,  $\mathbf{B}$  is the local large scale magnetic field, and  $C(f)$  represents CR scattering by small scale fluctuations in the magnetic field. In the local fluid rest frame,  $C(f)$  does not change the CR energy, but merely deflects its trajectory by diffusion in angle.  $\partial u/\partial x$  is zero everywhere except at the shock where it produces CR acceleration. Building on our experience of modelling laser-plasmas we solve the Vlasov-Fokker-Planck (VFP) equation by expressing the CR distribution function as a sum of spherical harmonics (Bell et al 2006).

$$f(x, \mathbf{p}, t) = \sum_{l,m} f_l^m(x, p, t) P_l^{|m|}(\cos \theta) e^{im\phi}$$

$$l = 0, \infty \quad m = -l, l \quad f_l^{-m} = (f_l^m)^*$$

where  $p_x = p \cos \theta$ ,  $p_y = p \sin \theta \cos \phi$  and  $p_z = p \sin \theta \sin \phi$ . The VFP equation can be separated into individual moment equations for the evolution of  $f_l^m(x, p, t)$ :

$$\begin{aligned} \frac{\partial f_l^m}{\partial t} + u \frac{\partial f_l^m}{\partial x} + c \left[ \frac{l-m}{2l-1} \frac{\partial f_{l-1}^m}{\partial x} + \frac{l+m+1}{2l+3} \frac{\partial f_{l+1}^m}{\partial x} \right] \\ - im \frac{ceB_x}{p} f_l^m + \frac{ceB_z}{2p} \beta_l^m \\ - p \frac{\partial u}{\partial x} \left[ \frac{(l-m)(l-m-1)}{(2l-3)(2l-1)} \left( \frac{\partial f_{l-2}^m}{\partial p} - (l-2) \frac{f_{l-2}^m}{p} \right) \right. \\ + \frac{(l-m)(l+m)}{(2l-1)(2l+1)} \left( \frac{\partial f_l^m}{\partial p} + (l+1) \frac{f_l^m}{p} \right) \\ + \frac{(l-m+1)(l+m+1)}{(2l+1)(2l+3)} \left( \frac{\partial f_l^m}{\partial p} - l \frac{f_l^m}{p} \right) \\ \left. + \frac{(l+m+1)(l+m+2)}{(2l+3)(2l+5)} \left( \frac{\partial f_{l+2}^m}{\partial p} + (l+3) \frac{f_{l+2}^m}{p} \right) \right] \\ - p \frac{u}{c} \frac{\partial u}{\partial x} \left[ \frac{l-m}{2l-1} \left( \frac{\partial f_{l-1}^m}{\partial p} - (l-1) \frac{f_{l-1}^m}{p} \right) \right. \\ \left. + \frac{l+m+1}{2l+3} \left( \frac{\partial f_{l+1}^m}{\partial p} + (l+2) \frac{f_{l+1}^m}{p} \right) \right] \\ = - \frac{l(l+1)}{2} \nu f_l^m \end{aligned} \quad (2)$$

where  $\beta_l^m = (l-m)(l+m+1)f_l^{m+1} - f_l^{m-1}$  for  $m > 0$  and  $\beta_l^0 = 2l(l+1)\Re(f_l^1)$ . The collision term  $C(f)$  on the right hand side reduces to an algebraic form because spherical harmonics are eigenfunctions of the Laplacian operator representing diffusion in  $\theta$  and  $\phi$ . The co-ordinate system has been chosen such that  $B_y = 0$  and  $\nu(x)$  is the collision frequency. The first three moment equations ( $l = 0, 1$ ) are

$$\begin{aligned} \frac{\partial f_0^0}{\partial t} + u \frac{\partial f_0^0}{\partial x} + \frac{c}{3} \frac{\partial f_1^0}{\partial x} - \frac{1}{3} \frac{\partial u}{\partial x} p \frac{\partial f_0^0}{\partial p} \\ - \frac{2}{15} \frac{\partial u}{\partial x} \left( p \frac{\partial f_2^0}{\partial p} + 3f_2^0 \right) - \frac{1}{3} \frac{u}{c} \frac{\partial u}{\partial x} \left( p \frac{\partial f_1^0}{\partial p} + 2f_1^0 \right) = 0 \end{aligned}$$

$$\begin{aligned} \frac{\partial f_1^0}{\partial t} + c \frac{\partial f_1^0}{\partial x} + 2\omega_z \Re(f_1^1) + \nu f_1^0 + u \frac{\partial f_1^0}{\partial x} + \frac{2c}{5} \frac{\partial f_2^0}{\partial x} \\ - \frac{\partial u}{\partial x} \left( \frac{3p}{5} \frac{\partial f_1^0}{\partial p} + \frac{1}{15} f_1^0 + \frac{6p}{35} \frac{\partial f_3^0}{\partial p} + \frac{24}{35} f_3^0 \right) \\ - \frac{u}{c} \frac{\partial u}{\partial x} \left( p \frac{\partial f_0^0}{\partial p} + \frac{2p}{5} \frac{\partial f_2^0}{\partial p} + \frac{6}{5} f_2^0 \right) = 0 \end{aligned}$$

$$\begin{aligned} \frac{\partial f_1^1}{\partial t} - i\omega_x f_1^1 - \frac{\omega_z}{2} \Re(f_1^0) + \nu f_1^1 \\ + u \frac{\partial f_1^1}{\partial x} + \frac{3c}{5} \frac{\partial f_2^1}{\partial x} - \frac{\partial u}{\partial x} \left( \frac{p}{5} \frac{\partial f_1^1}{\partial p} - \frac{1}{5} f_1^1 \right) \\ - \frac{\partial u}{\partial x} \left( \frac{12p}{35} \frac{\partial f_3^1}{\partial p} + \frac{48}{35} f_3^1 \right) - \frac{u}{c} \frac{\partial u}{\partial x} \left( \frac{3p}{5} \frac{\partial f_2^1}{\partial p} + \frac{9}{5} f_2^1 \right) = 0 \end{aligned} \quad (3)$$

where  $\omega_z = ceB_z/p$  and  $\omega_x = ceB_x/p$ . Supernova ejecta initially expand at velocities up to  $\sim c/5$ , and the SNR shock velocity decreases to  $\sim c/100$  during the first 1000 years. In the limit of small  $u/c$  the  $l = 0$  and  $l = 1$  equations dominate. In the Chapman-Enskog expansion, valid for scalelengths much larger than the CR scattering length, the magnitude of  $f_l^m$  decreases with increasing  $l$ , such that  $f_l^m \sim (u/c)^l f_0^0$ . With this expansion,  $f_l^m$  can be neglected for  $l > 1$ , in which case the above three equations ( $l = 0$  and  $l = 1$ ) reduce to

$$\begin{aligned} \frac{c}{3} \frac{\partial f_1^0}{\partial x} + u \frac{\partial f_0^0}{\partial x} = 0 \\ c \frac{\partial f_0^0}{\partial x} + 2\omega_z \Re(f_1^1) = -\nu f_1^0 \\ -i\omega_x f_1^1 - \frac{\omega_z}{2} f_1^0 = -\nu f_1^1 \end{aligned} \quad (4)$$

where  $f_0^0$  and  $f_1^0$  are real. The term  $u \partial f_0^0 / \partial x$  in the first equation cannot be neglected as small to order  $O(u/c)$  since  $f_0^0 \sim (c/u) f_1^0$ , but terms involving  $f_2^m$  are neglected since they are of order  $(u/c) f_1^m$ .  $f_1^m$  can be eliminated between the equations resulting in a diffusion equation for  $f_0^0$ .  $\partial u / \partial x$  is non-zero only at the shock, so the upstream diffusive solution of these equations for the CR density  $f_0^0$  for a general oblique shock is

$$f_0^0(x) = f_0^0(0) \exp(\kappa x) \quad \text{where} \quad \kappa = \frac{3\nu u_s}{c^2} \frac{\nu^2 + \omega_x^2 + \omega_z^2}{\nu^2 + \omega_x^2} \quad (5)$$

The corresponding CR fluxes are

$$f_1^0(x) = -\frac{3u_s}{c} f_0^0(x) \quad \text{and} \quad f_1^1(x) = -\frac{3u_s}{2c} \frac{(\nu + i\omega_x)\omega_z}{\nu^2 + \omega_x^2} f_0^0(x) \quad (6)$$

An alternative tensor notation (Johnston 1960) expresses the CR distribution function to first order in  $u/c$  as  $f = f_0 + \mathbf{f}_1 \cdot \mathbf{p}/p$ . The tensor expansion is related to the spherical harmonic expansion by  $f_x = f_1^1$ ,  $f_y = -\Re\{2f_1^1\}$ , and  $f_z = \Im\{2f_1^1\}$ . We choose the  $y$  and  $z$  directions such that  $B_y = 0$ . In this geometry,  $f_x$  is parallel to the shock normal,  $f_z$  is perpendicular to the shock normal and lies in the plane containing the magnetic field and the shock normal, and  $f_y$  is perpendicular to both the shock normal and the magnetic field.  $f_1^0$ , or  $f_x$ , represent CR diffusion parallel to the shock normal. CR drift along the magnetic field is represented by

a combination of  $f_1^0$  and  $\Im\{f_1^1\}$ . Both real and imaginary parts of  $f_1^1$  are zero everywhere for a parallel shock.

Downstream of the shock ( $x > 0$ ), the corresponding solution to the same equations is that for a uniform isotropic CR distribution at rest with respect to the background plasma:  $f_0^0(x) = f_0^0(0)$ ,  $f_1^0 = f_1^1 = 0$  where  $f_0^0(0)$  is the CR density at the shock. Matching the upstream and downstream CR distribution functions at the shock requires  $f_0^0$  to be continuous at the shock. Integrating the ( $l = 1, m = 0$ ) moment equation across the shock requires  $f_1^0 - (u/c)p\partial f_0^0/\partial p$  to be continuous at the shock. The term  $-(u/c)p\partial f_0^0/\partial p$  arises from the frame transformation across the shock. Assuming a strong shock in which  $u = u_s/4$  downstream, the upstream flux  $f_1^0 - (u_s/c)p\partial f_0^0/\partial p$  must equal the downstream flux  $-(u_s/4c)p\partial f_0^0/\partial p$ , giving  $p\partial f_0^0/\partial p = -4f_0^0$  from equation (6). This leads to the well-known power law  $f_0^0 \propto p^{-4}$ , equivalent to  $n(E) \propto E^{-2}$  for CR acceleration at a strong shock. This solution is correct in the limit of low shock velocity for a parallel shock in which  $B_y = B_z = 0$ .

The  $f_0^0$  and  $f_1^m$  components of the distribution function can be matched across a parallel shock. However, it is not possible to match the solution for  $f_1^1$  across an oblique shock when the higher order terms ( $f_l^m$  for  $l > 1$ ) are neglected. The Chapman-Enskog expansion breaks down because of the abrupt gradient at the shock. In the limit of small shock velocity, the mismatch at an oblique shock is unimportant and introduces only a correction of order  $u/c$  to the solution. Consequently, the spectrum at an oblique shock is still  $f_0^0 \propto p^{-4}$  in the low velocity limit, but the corrections of order  $u/c$  become important at the expansion velocities of young SNR. The corrections are more important for oblique shocks than for parallel shocks for which the corrections are of order  $(u/c)^2$ . As we show below, the CR spectrum is expected to deviate from  $p^{-4}$  more strongly for oblique shocks than for parallel shocks.

One reason why oblique shocks deviate more strongly from a  $p^{-4}$  spectrum is that the expansion parameter is more correctly  $u/(c\cos\theta)$  rather than  $u/c$ , where  $\theta$  is the angle between the magnetic field and the shock normal. CR diffuse away from the shock along magnetic field lines at the angle  $\theta$  to the shock normal. If  $u > c\cos\theta$ , it is impossible for CR to escape upstream of the shock by streaming along field lines. Shocks with a velocity  $u$  exceeding  $c\cos\theta$  are accounted ‘superluminal’, even if the shock velocity is in fact considerably less than the speed of light. Corrections to the spectral index  $\gamma$ , where  $f_0^0(0) \propto p^{-\gamma}$ , are especially strong when  $u/\cos\theta$  approaches  $c$ .

The aim of this paper is to calculate the CR spectral index at oblique shocks at shock velocities relevant to young SNR. Integration of the first of equations (3) from far upstream to far downstream gives

$$\gamma = \frac{\int_{-\infty}^{\infty} (3f_0^0 + 6f_2^0/5 + 2uf_1^0/c) (\partial u/\partial x) dx - 3u(\infty)f_0^0(\infty)}{\int_{-\infty}^{\infty} (f_0^0 + 2f_2^0/5 + uf_1^0/c) (\partial u/\partial x) dx} \quad (7)$$

where  $u(\infty)$  and  $f_0^0(\infty)$  are the values of  $u$  and  $f_0^0$  far downstream. At the shock  $f_0^0(0) \propto p^{-\gamma}$ . To leading order in  $u/c$ , and for a discontinuous shock transition

$$\gamma = 3 + \frac{3u(\infty)}{u_s - u(\infty)} \frac{f_0^0(\infty)}{f_0^0(0)} \quad (8)$$

where  $f_0^0(0)$  is the value of  $f_0^0$  at the shock. For a shock compression of 4 ( $u(\infty) = u_s/4$ ),  $\gamma = 4$  since the downstream CR density is uniform ( $f_0^0(\infty) = f_0^0(0)$ ) to order  $u/c$ . We shall show that for an oblique shock,  $f_0^0(\infty) \neq f_0^0(0)$ , and  $\gamma$  differs from 4 to order  $u/c$ .

The ratio  $f_0^0(\infty)/f_0^0(0)$  is important for determining the spectral index  $\gamma$  because  $f_0^0(0)$  determines the rate at which CR are accelerated by crossing and recrossing the shock, while  $f_0^0(\infty)$  determines the rate at which CR are advected away from the shock downstream. The spectral index is determined by the number of times CR cross the shock before escaping downstream. Hence  $\gamma$  depends on  $f_0^0(\infty)/f_0^0(0)$ , although the values of  $f_1^0$  and  $f_2^0$  at the shock can also change the spectral index to higher order as evident in equation (7).

### 3 NUMERICAL MODEL

For all except the highest energy CR, the acceleration time is shorter than the time for which the shock exists, so we seek a time-independent solution with  $\partial f_l^m/\partial t = 0$  for all  $l$  and  $m$ . We assume that the collision frequency  $\nu$  due to CR scattering by small scale magnetic field is proportional to the local CR Larmor frequency:

$$\nu(x) \propto |\mathbf{B}(x)| \quad (9)$$

where  $\mathbf{B}$  is the local magnetic field, thus making the ratio of the CR mean free path to the Larmor radius the same both upstream and downstream of the shock. By definition of  $\nu$  as a frequency for small angle scattering, the coefficients  $f_l^m$  decay exponentially at a rate  $[l(l+1)/2]\nu$  in the absence of all other effects. The large-scale magnetic field is assumed to be uniform in the upstream plasma,  $B_x = B_0 \cos\theta$ ,  $B_y = 0$ ,  $B_z = B_0 \sin\theta$  and compressed by the shock to give a uniform downstream field,  $B_x = B_0 \cos\theta$ ,  $B_y = 0$ ,  $B_z = 4B_0 \sin\theta$ . As already stated, we assume throughout that the plasma is compressed by a factor 4 at the shock, even at high shock velocity where the compression is in reality increased by the reduced relativistic ratio of specific heats.

From the self-similar structure of equation (2) it can be shown that the steady state CR distribution function is a power law in momentum at the shock. The shock is the only point in space at which  $\partial u/\partial x$  is non-zero, and hence the only point at which  $f(x, p)$  is connected to the values of  $f(x, p + \Delta p)$  and  $f(x, p - \Delta p)$ . If the spectral index at the shock is  $\gamma$ ,  $p\partial f_l^m/\partial p$  can be replaced by  $-\gamma f_l^m$  in equation (2) so that it becomes an equation with differentials in  $x$  but not  $p$ .  $p$  only appears in combination with the magnetic field as  $eB_x/p$  and  $eB_z/p$  as the inverse of the CR Larmor radius by which all distances are scaled. The objective of the calculation is then to find the value of  $\gamma$  for which the boundary conditions are  $f_l^m = 0$  for all  $l, m$  far upstream where  $x \rightarrow -\infty$ , and for which only  $f_0^0$  is non-zero far downstream. Downstream,  $f_l^m \rightarrow 0$  as  $x \rightarrow \infty$  for  $l > 0$ .

The steady state VFP equation is non-linear because of the multiplication of the two unknowns  $f$  and  $\gamma$  in terms proportional to  $p\partial f_l^m/\partial p = -\gamma f_l^m$ . Making the replacement  $p\partial f_l^m/\partial p = -\gamma f_l^m$ , we iterate to a steady state solution by restoring the time-derivative in equation (2), fixing the value of  $f_0^0$  at the shock, and improving the value of  $\gamma$  as equation (2) is integrated forward in time until a steady state is reached in which CR advect at constant density

through a computational boundary placed far downstream of the shock. During the time integration,  $\gamma$  is calculated at each timestep from equation (7). Equation (2) is solved in finite difference form with  $f_l^m$  defined at the cell centres for even  $l$ , and defined on the cell boundaries for odd  $l$ . All spatial derivatives are then naturally centre-differenced. A stretched spatial grid is used to give fine resolution near the shock, where  $f_l^m$  changes rapidly on scales less than a CR Larmor radius. A coarser resolution is used at large distances from the shock where  $f_l^m$  changes on the scale-length of the shock precursor. The background fluid velocity  $u$  is pre-determined and changes smoothly by a factor of four across a thin shock transition.  $\mathbf{B}$  is determined by the flux freezing condition. At the shock, we impose the form  $u = 0.625u_s - 0.375u_s \tanh(x/x_s)$ . For high shock velocity  $u_s = c/5$ , the lengthscale  $x_s$  for the shock transition is set to 0.01 times the upstream CR Larmor radius, and the spacing of the computational grid at the shock is set to  $\Delta x = x_s/3$ . As shown in figure 1(a), halving  $\Delta x$  makes very little difference in the case requiring the highest resolution (a perpendicular shock with  $u_s = c/5$ ).  $x_s$  and  $\Delta x$  are set a factor of two larger for low shock velocities where the natural scalelengths are larger. For quasi-perpendicular high velocity shocks ( $u_s = c/5$ ), the spherical harmonic expansion was extended to  $l = 11$ . Test calculations with a larger number,  $l = 15$ , made negligible difference to the results.

With our neglect of non-linear hydrodynamic effects due to the CR pressure in the precursor, the shock transition takes place over a distance very much less than the Larmor radius of high energy CR. For this reason our chosen scale-length  $x_s$  is much smaller than the Larmor radius. However we cannot treat the shock as a discontinuity since  $\partial u/\partial x$  would then be infinite which is not possible in our numerical treatment. An alternative numerical method would be to treat the shock as a discontinuity with a matrix relating the values of  $f_l^m$  each side of the shock,  $f_{l_1}^m = A_{l_1 l_2}^m f_{l_2}^m$ .  $A_{l_1 l_2}^m$  would be a full matrix in  $(l_1, l_2)$  with the spherical harmonic expansion extended to very high order. A discontinuous shock introduces high order harmonics, making this approach unrealistic. Smoothing the shock over a small distance  $x_s$  terminates the harmonic expansion without significantly changing the spectral index. However, as an additional check on the overall accuracy of the code (Code A), we wrote a completely separate code (Code B) which treats the shock jump differently, allowing a sharper transition at the cost of dispensing with second order terms in  $u/c$  at the shock. Code B solves the reduced equations

$$\frac{\partial f_l^m}{\partial t} + u \frac{\partial f_l^m}{\partial x} + c \left[ \frac{l-m}{2l-1} \frac{\partial f_{l-1}^m}{\partial x} + \frac{l+m+1}{2l+3} \frac{\partial f_{l+1}^m}{\partial x} \right] - im \frac{ceB_x}{p} f_l^m + \frac{ceB_z}{2p} \beta_l^m - S_l^m = -\frac{l(l+1)}{2} \nu f_l^m$$

where

$$S_0^0 = \frac{1}{3} \frac{\partial u}{\partial x} p \frac{\partial f_0^0}{\partial p} \quad \text{and} \quad S_2^0 = \frac{2}{3} \frac{\partial u}{\partial x} p \frac{\partial f_0^0}{\partial p} \quad (10)$$

and all other  $S_l^m = 0$ .  $S_2^0$  must be included because it balances the jump in  $f_1^0$  across the shock. All other terms involving  $\partial u/\partial x$  are smaller to order  $u/c$  but not negligible. Their omission substantially simplifies the numerical integration across the shock. Some minimal smoothing of the shock transition on the scale of the computational grid is

still included to allow the spherical harmonic expansion to be terminated. The output from the code B is compared with the results from the main code (code A) in figure 2(b) for  $\nu/\omega_g = 0.1$  and  $u/c = 0.1$ , which we consider to be a representative ‘standard’ set of parameters. As expected, the comparison shows a difference in the spectral index due to the neglect of second order terms in  $u/c$ , but the two curves are sufficiently close to give confidence that the results from Code A can be relied upon.

## 4 RESULTS

Equation (2) was solved for a variety of shock velocities,  $u_s = c/5$ ,  $c/10$  &  $c/30$ , and a variety of collisionalities,  $\nu/\omega_g = 0.03$ ,  $0.1$ ,  $0.3$  &  $1.0$ , where  $\omega_g = ceB_0/p$  is the CR Larmor frequency in the upstream plasma. The spectral indices  $\gamma$  are plotted in figure 1 as a function of  $\cos\theta$  where  $\theta$  is the angle between the shock normal and the magnetic field. At a perpendicular shock  $\cos\theta = 0$ . At a parallel shock  $\cos\theta = 1$ . In the case of a shock advancing into a randomly disordered magnetic field  $\cos\theta$  is uniformly distributed between 0 and 1. Also plotted on the vertical axis is the synchrotron spectral index  $\alpha = (\gamma - 3)/2$ .

The results can be summarised as follows:

- 1) In the case of parallel shocks, the CR spectral index deviates little from  $\gamma = 4$  ( $\alpha = 0.5$ ).
- 2) The quasi-parallel spectrum is flattened ( $\gamma < 4$ ,  $\alpha < 0.5$ ).
- 3) The quasi-perpendicular spectrum is steepened ( $\gamma > 4$ ,  $\alpha > 0.5$ ) and CR are accelerated less efficiently.
- 4) Deviation from  $\gamma = 4$  is strongest for high shock velocity, but significant deviations are still present at velocities as low as  $10,000 \text{ km sec}^{-1}$ .
- 5) Deviations from  $\gamma = 4$  are greater if the angular scattering time is much longer than the CR Larmor gyration time ( $\nu \ll \omega_g$ ).
- 6) In the case of a shock advancing into a magnetic field which is disordered on scales both larger and smaller than a CR Larmor radius, the spectral index averages to  $\gamma = 4$  since the mean value of  $\gamma$  averaged over  $\cos\theta$  is close to  $\gamma = 4$  (see figure 1).
- 7) The overall spectral index can only be strongly flattened if the shock is predominantly quasi-parallel. Conversely, it can only be strongly steepened if the shock is predominantly quasi-perpendicular.

The magnitude of spectral index deviation from  $\gamma = 4$  depends strongly on the ratio of the CR scattering frequency  $\nu$  to the CR Larmor frequency  $\omega_g$ . The parameter  $\nu/\omega_g$  is poorly known both observationally and theoretically, but there are reasons for assuming that for SNR shocks  $\nu/\omega_g$  lies in the band of values we choose for figure 1. Very low collision frequencies ( $\nu/\omega_g \ll 1$ ) can be ruled out for SNR shocks because CR acceleration would then be too slow for CR acceleration to PeV energies as required by the galactic CR spectrum. At the opposite limit, large collision frequencies ( $\nu/\omega_g > 1$ ) can probably be ruled out since  $\nu/\omega_g > 1$  would correspond to fields with no large scale structure. This is unlikely because some form of power-law magnetic field turbulence spectrum can be expected which includes fluctuations at wavenumbers less than, as well as greater than, the inverse of any particular CR Larmor radius. As a guess,

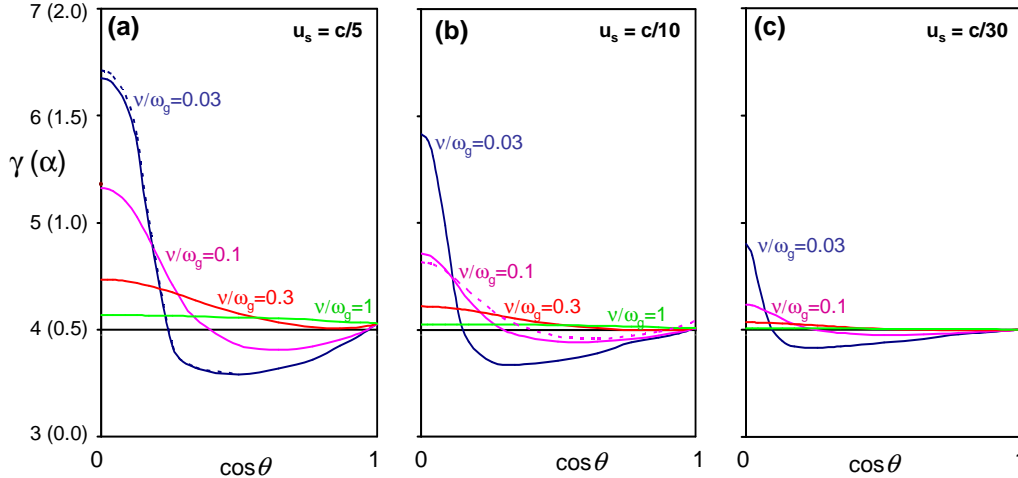


**Figure 1.** Spectral indices at three shock velocities ( $c/5$ ,  $c/10$ ,  $c/30$ ) and four CR scattering rates ( $\nu/\omega_g = 0.03$ ,  $0.1$ ,  $0.3$  and  $1.0$ ).  $\gamma$  is the CR energy spectral index.  $\alpha$  is the corresponding electron synchrotron spectral index,  $\alpha = (\gamma - 3)/2$ .  $\theta$  is the shock obliquity. At a perpendicular shock  $\cos\theta = 0$ . At a parallel shock  $\cos\theta = 1$ . The dotted line in 1(a) next to the curve for  $\nu/\omega_g = 0.03$  is a calculation with finer spatial resolution with  $\Delta x$  halved as an accuracy check on the most demanding calculation. The dotted line in 1(b) next to the curve for  $\nu/\omega_g = 0.1$  is a comparison calculation with code B. All other curves are calculated with Code A.

and it is little more than that at present, it seems reasonable to suppose that anisotropic CR drifts ( $f_x$ ,  $f_y$  &  $f_z$ ) might decay by a factor of two in the time it takes for a CR to make one gyration through an angle of  $2\pi$ . This corresponds to  $\nu/\omega_g = 0.11$ . It is often presumed that ‘Bohm diffusion’ applies to CR scattering, but this can variously and ambiguously be taken to mean  $\nu/\omega_g = 1$ ,  $\nu/\omega_g = 1/3$  or  $\nu/\omega_g = 0.125$  as in the NRL Plasma Formulary (Huba 1994).  $\nu/\omega_g = 1$  would seem to be too large because drift anisotropies then decay by a factor of  $\sim \exp(-2\pi) = 10^{-3}$  during one CR gyration time, which would only be possible if the magnetic field responsible for small scale scattering is much greater than the field structured on the scale of a CR Larmor radius. The value of the ratio  $\nu/\omega_g$  is a major uncertainty in our discussion, and we take  $\nu/\omega_g = 0.1$  as a ‘standard’ value.

Figure 2 displays profiles of  $f_0^0$ ,  $f_1^0$  and  $f_1^1$  for a parallel shock ( $\theta = 0^\circ$ ), an oblique shock ( $\theta = 60^\circ$ ), and a perpendicular shock ( $\theta = 90^\circ$ ). Figure 3 shows the detailed profiles in the immediate environment of the shock

for  $\theta = 60^\circ$ ,  $72^\circ$ , &  $90^\circ$ . In figures 2 and 3,  $\nu/\omega_g = 0.1$  and  $u_s = c/10$ . The oblique shock ( $\theta = 60^\circ$ ) exhibits a peak in the CR density at the shock as previously identified in mildly relativistic shocks. Geissler et al (1999) convincingly argued for a build-up of CR immediately upstream of the shock because CR approaching the shock from upstream with certain pitch angles are unable to cross the shock into the downstream region. Similar structures are evident in Monte Carlo calculations by Ellison et al (1996). Figure 3 is a plot of CR density profiles at higher resolution. At  $\theta = 60^\circ$  an excess of CR is seen within one CR Larmor radius both upstream and downstream of the shock. According to equations (7) and (8), as discussed above, the excess CR density at the shock results in enhanced CR acceleration. The excess increases the rate at which CR cross the shock, and hence increases the probability of acceleration to high energy before being advected away downstream of the shock. This explains the flattening of the CR spectrum at quasi-parallel shocks as seen in figure 1.

The CR density profile at a perpendicular shock is dif-

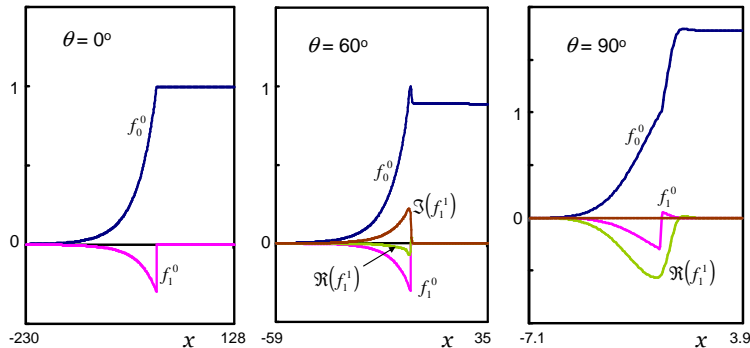


**Figure 2.** Spatial profiles of  $f_0^0$ ,  $f_1^0$ ,  $\Re\{f_1^1\}$ , and  $\Im\{f_1^1\}$  for a parallel shock, an oblique shock at  $\theta = 60^\circ$  and a perpendicular shock.  $\nu/\omega_g = 0.1$  and  $u_s = c/10$ . The spatial distance  $x$  from the shock at  $x = 0$  is measured in CR Larmor radii. The vertical axis is scaled such that  $f_0^0 = 1$  at the shock.

ferent as seen in Figure 2(c) and in figure 3. Diffusion theory can still be applied to CR at a perpendicular shock by deconstructing the CR trajectory into diffusive motion of the gyrocentre and gyration about the gyrocentre. The gyratory part of the trajectory acts as a spatial convolution on the motion of the gyrocentre. This spreads the CR trajectory over a distance of one Larmor radius and smooths the CR density at the shock. A discontinuous jump in CR density is not possible at the shock on a scale less than a Larmor radius. Correspondingly, figures 2(c) and 3 exhibit a CR density gradient both downstream and upstream of a perpendicular shock. Consequently, the CR density precisely at the shock is smaller than the CR density far downstream. In this case, the rate at which CR cross the shock is reduced and the spectrum at quasi-perpendicular shocks is steeper than  $p^{-4}$  in line with equations (7) and (8). According to equations (9) and (10) of Jokipii (1987) the diffusive approximation is only valid at a quasi-perpendicular shock when  $\nu/\omega_g > u_s/c$ . This is consistent with the results shown in our figure 1 where we see that deviations from a  $p^{-4}$  spectrum occur where this condition is not met.

The profile for  $\theta = 72^\circ$  is intermediate between the quasi-perpendicular and the quasi-parallel cases. The steep-

ening and flattening effects are both present but cancel out to leave a CR density approximately equal to that far downstream and a CR spectrum proportional to  $p^{-4}$ .

## 5 OBSERVATIONS

### (i) Galactic cosmic rays

CR arriving at the earth with energies up to a few PeV conform to a remarkably straight power law spectrum  $p^{-\gamma}$  with  $\gamma$  equal to 4.6-4.7. The more rapid escape from the galaxy of high energy CR steepens the spectrum, but this cannot be solely responsible for steepening the spectrum from an index at source of  $\gamma = 4.0$ . The underlying CR source spectrum probably has an index between about 4.2 and 4.3 (Gaisser, Protheroe & Stanev 1998, Hillas 2005). Figure 1 indicates that the oblique-shock effects discussed here can produce a steepened spectrum ( $\gamma > 4$ ) at high shock velocities, but only if the shock has a tendency towards a quasi-perpendicular rather than quasi-parallel configuration. As discussed in section 4, the spectral index averaged over random magnetic field orientations is approximately the same as for the low velocity limit:  $\gamma = 4$ .

The shock might be preferentially quasi-perpendicular

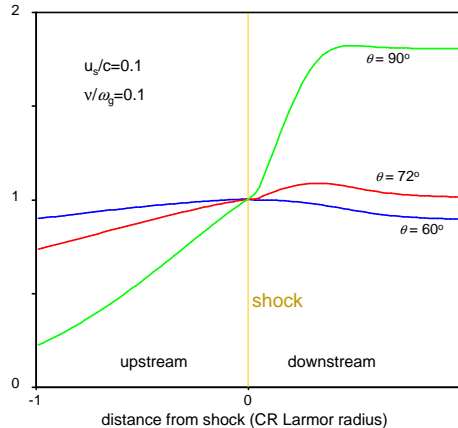


**Figure 3.** Spatial profiles of the CR density  $f_0^0$  within one CR Larmor radius either side of the shock.  $v/\omega_g = 0.1$  and  $u_s = c/10$ .

in the event of strong magnetic field amplification in the precursor due to CR streaming (Bell 2004, 2005). Field amplification is driven by  $\mathbf{j}_{CR} \times \mathbf{B}$  where  $\mathbf{j}_{CR}$  is the electric current carried by streaming CR and  $\mathbf{B}$  is the local magnetic field. The plasma is set in motion perpendicular to  $\mathbf{j}_{CR}$  and therefore predominantly perpendicular to the shock normal since  $\mathbf{j}_{CR}$  is directed away from the shock. These upstream fluid motions stretch the magnetic field perpendicular to the shock normal producing a quasi-perpendicular shock orientation as evident in the sample field lines shown in figure 4 of Bell (2005). Hence strong field amplification can be expected to lead preferentially to a quasi-perpendicular shock geometry and the steepening of the spectral index. This is not contradicted by polarimetric observations which suggest a predominantly radial magnetic field in SNR. Zirakashvili & Ptuskin (2008) point out that this field orientation probably develops downstream of the shock due to differential fluid motions after the plasma has passed through the shock. A similar effect is seen in simulations by Giacalone & Jokipii (2007). Alternatively, the shock might be preferentially quasi-perpendicular if the supernova expands into a pre-existing circumstellar wind supporting a magnetic field in the form of a Parker spiral. This would be unsurprising since SN are often preceded by strong mass loss.

Another possible source of spectral steepening is non-linear feedback onto the shock hydrodynamics (Drury & Völk 1981, Drury 1983). Non-linear effects produce a concave spectrum which is steepened at low energy but flatter than  $p^{-4}$  at high energy (Bell 1987, Falle & Giddings 1987). Allen et al (2008) find evidence for concavity in the synchrotron spectrum of SN1006. The galactic CR spectrum is not noticeably concave, but a compensating convexity due to momentum-dependent escape from the galaxy could produce the measured spectrum. The CR spectrum could be the result of a complicated mixture of non-linear, oblique-shock and escape effects.

#### (ii) Young supernova remnants

Further evidence for deviation from a  $p^{-4}$  CR source spectrum can be found in synchrotron spectra. SNR radio spectral indices can deviate considerably from  $\alpha = 0.5$  ( $\gamma = 4$ ). Since synchrotron loss times at radio wavelengths are longer than the dynamical time, the measured spectral index gives a proper indication of the cosmic ray source spectrum. Observations show that young pre-Sedov SNR consistently exhibit radio spectral indices significantly steeper than  $\alpha = 0.5$ . Either magnetic field amplification or expansion into a Parker spiral may produce a geometry favouring quasi-perpendicular shocks and spectral steepening. But in either case, a high shock velocity is needed. If this is the explanation of the steeper than expected galactic CR spectrum, then it implies that galactic CR are accelerated by young SNR rather than by SNR in the Sedov phase.

In Figure 4 we plot a sample of SNR (see Table 1) and their spectral indices as a function of shock velocity. It is related to the analysis of Glushak (1985) who plotted the spectral indices of young shell SNR against SNR age to show that the spectra flattened with time. Here we plot the spectral index against the *mean* expansion velocity  $v_{sh}$  calculated as the mean radius divided by SNR age, and extend and update the sample of SNR. We take the mean rather than the momentary expansion velocity since the overall spectrum is an addition of cosmic rays that were accelerated throughout the entire age of the remnant. Depending on the number of cosmic rays that enroll in the acceleration process early versus late, additional differences in the spectral index can result. The average time since acceleration would be different for core-collapse SNR and Type Ia SNe. In Type Ia SNe most CR are accelerated at late times as the shock expands into a uniform medium, whereas CR acceleration is more evenly spread in the case of core-collapse SNR which expand into a  $r^{-2}$  density profile of a circumstellar wind (Schure et al 2010).

The Galactic remnants in figure 4 were taken from the updated online catalogue by Green (2009). They were selected if they were classified as having a clear shell morphology (i.e. no contamination in radio from a central source), had a measured spectral index and a readily available distance estimate. Only sources were selected that are estimated to be younger than 10,000 yr, and not clearly interacting or overlapping with other radio sources.

Because of a lack of data for galactic SNR with ages less than 200 years, we turn to the extragalactic remnants of recent SN for data on very young SNR. We added data for SN1987A (Manchester et al 2002, Manchester et al 2005) and SN1993J (Weiler et al 2007), and a sample of Type Ib/c supernovae taken from Chevalier & Fransson (2006). Two data points are plotted for SN1987A corresponding to observations in 2002 and 2005 since its expansion velocity slowed significantly between these years.

For our purpose, very young SNR from Type Ib/c SNe are especially interesting because of their high expansion velocities. They do not necessarily reflect a statistical sample. Their expansion velocities are based on models of the radius of the remnant at the time of the peak in synchrotron self absorption, as described in (Chevalier 1998). Each of the Type Ib/c's has a steep spectral index except for SN1998bw which was the only one to be associated with a GRB. Chevalier & Fransson (2006) argue that the flattening with time may be a result of the nonlinear feedback of the cosmic rays in the plasma, which weakens with time. Nonlinear models by Ellison & Reynolds (1991) can partly account for the steepening, up to  $\alpha \approx 0.8$ , if the cosmic ray pressure constitutes a dominant fraction. The total steepening may be a cumulative effect of non-linear and oblique-shock steepening.

Except in the cases of the historical supernova remnants, the age of the galactic remnants is a highly uncertain parameter. Often it is based on the distance measurement, giving the size of the remnant, and from the temperature in X-rays a shock velocity is derived. Subsequently a Sedov model is used to arrive at the age estimate. However, in addition to uncertainties in the size, if any energy is lost in e.g. cosmic rays the shock velocity may be severely underestimated, as was shown might be the case in RCW 86 (Helder et al 2009). The data points in Figure 4 should therefore be considered with large error bars in  $v_{\text{sh}}$  and are likely to underestimate the shock velocity on average. The ones for which this is known are indicated with an arrow, however this does not mean that other data points are necessarily more certain. Occasionally the shock velocity can possibly be overestimated when the age measurement is based on the age of the associated pulsar (i.e. G292.2-0.5). The age of the historical remnants is obviously more certain. However, their distance estimate may still introduce a large uncertainty in the size and shock velocity. Nevertheless, the data show a clear trend. As a guide, we plot on figure 4 a trend-line:

$$\alpha = 0.7 + 0.3 \log_{10}(v_{\text{sh}}/10^4 \text{km s}^{-1})$$

where  $v_{\text{sh}}$  is the radius divided by age for SNR. Although the data are uncertain at high velocity, the rise in the spectral index levels off at about  $\alpha = 1$ . A levelling off also occurs at  $\alpha \sim 0.5$  for older SNR with lower expansion velocities. A better fit to the overall data may be an S-shaped curve with a stronger increase of spectral index at velocities around

$10^4 \text{km s}^{-1}$ . An appropriate trend-line for the historical SNR, for which the velocity estimates are more reliable, is

$$\alpha = 0.7 + 0.8 \log_{10}(v_{\text{sh}}/10^4 \text{km s}^{-1})$$

as plotted in figure 4.

The two data points for SN1987A show that the variation of spectral index with shock velocity is exhibited within the lifetime of a single SNR. The radio spectrum of Cassiopeia A has similarly been observed to flatten with time as already argued in the seventies (Baars et al 1977). A flattening of the Cas A radio spectrum from  $\alpha = 0.79$  to  $\alpha = 0.77$  was found over a period of 15 years (1965–1980). Further flattening was confirmed by O’Sullivan & Green (1990), although they found it proceeding at a slower rate.

### (iii) Spectral index variations within SNR

Further signatures of spectral index variation with shock obliquity may be visible in SNR expanding at high velocity into a uniform magnetic field. If magnetic field amplification is weak, the field orientation at the shock is that of the pre-existing interstellar field. The electron spectrum should be flatter where the shock is quasi-parallel, increasing the number of CR electrons accelerated to high energy, and producing stronger X-ray synchrotron emission at the poles.

Detailed, resolved, spectra are available for the remnant of SN1006. This image shows a distinct bipolar symmetry, which is thought to reflect the directionality of the ambient magnetic field. Most likely the bright caps are the parts where the shock velocity is parallelly aligned with the background magnetic field (Rothenflug et al 2004, Bocchino et al 2011). In an analysis of the combined radio- with the X-ray spectrum Allen et al (2008) found evidence for hardening of the spectrum in this area, both for models which included curvature in the spectrum and those without. The fractional hardening is modest but significant. The magnetic field in SN 1006 is generally believed to be not much amplified and therefore plausibly reflects the original field geometry. The spectral steepening towards the fainter parts, i.e. higher obliquity angle between the shock normal and magnetic field lines, is consistent with our findings.

Detailed data are also available for Tycho’s SNR, as was presented in Katz-Stone (2000). This remnant shows a much more patchy profile in radio. Spectra were extracted from various parts over the remnant. No clear trend with position was found. However, it was argued that the brightest parts have a flatter spectral index than the steeper parts, which is a similar trend to that in SN1006.

A spatially resolved study of the radio spectrum of Cassiopeia A (Wright et al 1999) shows variation of the spectral index with position in the remnant. Generally, a steeper power law is found in the outermost regions, whereas in the inner bright ring the spectral index is flatter (although still  $\alpha > 0.75$ ). The spectra they found do not show signs of spectral curvature and seem to be coherent over larger scales than the diffusion scale. This indicates a common mechanism, such as e.g. a preferentially perpendicular field at the forward shock might be able to account for. The magnetic field in Cas A is strongly amplified and thus a preferentially perpendicular field may be expected.

### (iv) Older supernova remnants

The radio spectral indices of old SNR in the self-similar Sedov phase are usually around 0.5, but many have flatter spectra which may be due to additional second order Fermi acceleration in MHD turbulence (Ostrowski 1999), or possibly due to compression ratios greater than four at radiative shocks. Because the shock velocities are much lower than in young SNR, the oblique-shock effects considered in this paper are unlikely to contribute to the flattening of the spectral index.

## 6 CONCLUSIONS

We have shown that a wide range of spectral indices are possible for shock velocities of around  $c/30$  or higher. The CR spectrum is steepened for quasi-perpendicular shocks and flattened for shocks closer to parallel geometry. This may present a natural explanation of why few observed energetic particle spectra conform to the non-relativistic test-particle  $\gamma = 4$  spectrum, although non-linear effects and second order Fermi acceleration probably also play a role. For a shock propagating into a randomly orientated upstream magnetic field the steepening and flattening of the spectrum averages out to produce  $\gamma = 4$ . Observed radio spectra show that the spectrum is steeper at high shock velocity which suggests that high velocity shocks tend to be quasi-perpendicular rather than parallel. A predominantly quasi-perpendicular configuration may arise if magnetic field amplification is strong as expected at high shock velocity. Alternatively, a quasi-perpendicular geometry may result from expansion into a circumstellar wind supporting a Parker spiral.

The galactic CR energy spectrum and the radio spectra of young SNR require a CR spectrum at source which is steeper than  $p^{-4}$ . The galactic CR spectral index may be explained if CR are accelerated by shocks such as those found in the historical SNR. These SNR have a relatively large shock area, still expand at a relatively high velocity into a possibly dense circumstellar medium, and produce CR with a suitable spectral index if the SNR shock is predominantly quasi-perpendicular. The spectral index is sensitive to the CR scattering rate  $\nu$  which is presently not well determined by observation or theory. Observations (figure 4) suggest a fairly clear relation between SNR shock velocity and spectral index.

Our model depends on the presumed simplification that the magnetic field structure can be separated into a small scale disordered component that scatters CR through small angles, and a large scale component which is uniform over a CR Larmor radius. However, the essential reason for spectral steepening by quasi-perpendicular shocks is that the magnetic field sweeps CR through the shock making it difficult for CR to return to the shock for further acceleration. This effect can be expected to be independent of the detailed field structure. Another realisation of a related effect would be spectral steepening due to field line wandering (Kirk, Duffy & Gallant 1996).

## 7 ACKNOWLEDGEMENTS

The research leading to these results has received funding from the European Research Council under the European

Community's Seventh Framework Programme (FP7/2007-2013) / ERC grant agreement no. 247039 and from grant number ST/H001948/1 made by the UK Science Technology and Facilities Council. We especially thank John Kirk of MPIK Heidelberg for very helpful discussions.

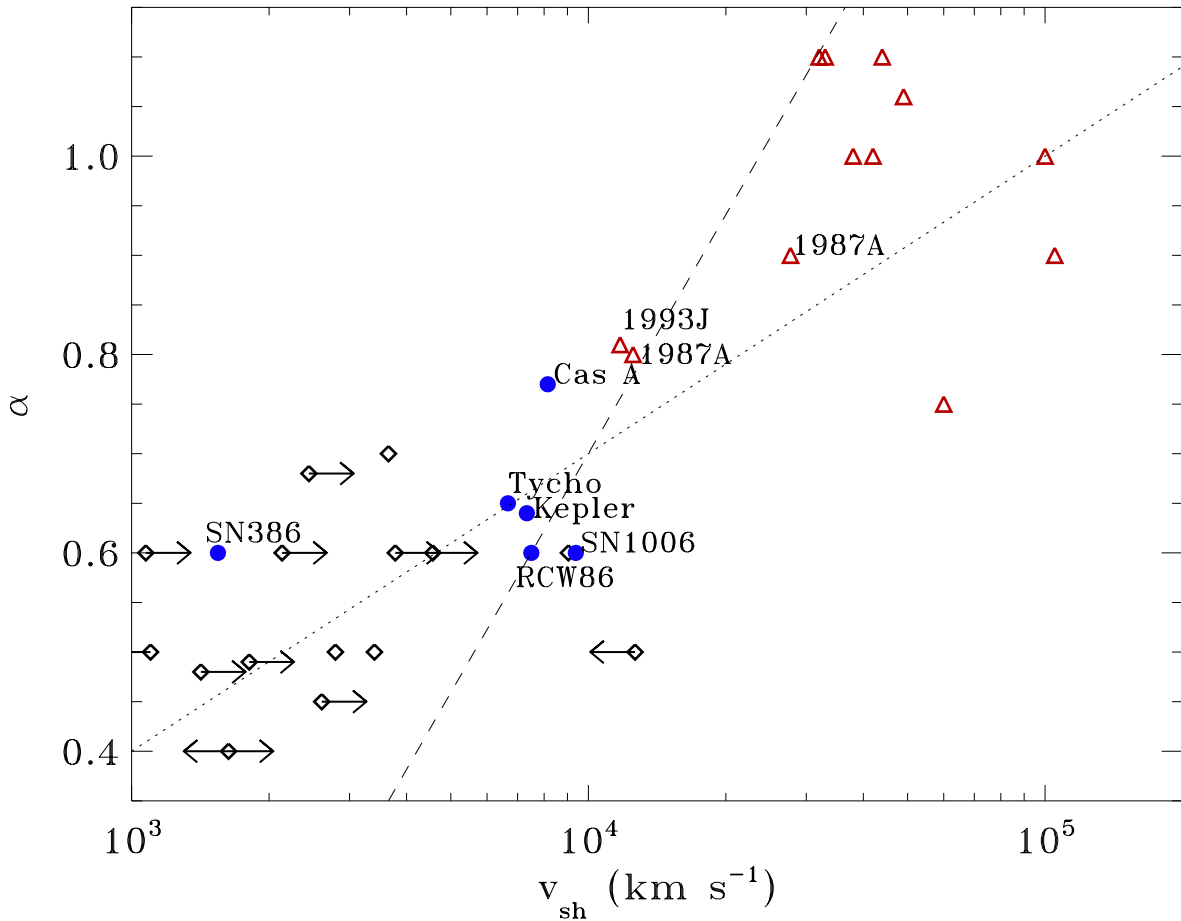


**Figure 4.** Synchrotron spectral index versus shock velocity for galactic (black diamonds), historic (blue filled circles), and extragalactic SNR and SNe (red triangles), as given in Table 1. The arrows indicate known issues with distance and / or age estimates and the likely limit derived from that in shock velocity. Note that there remain large errors in  $v_{\text{sh}}$  also for the other data points. The dashed line shows the trend in spectral index that is biased towards the historical galactic remnants  $\alpha = 0.7 + 0.8 \log_{10}(v_{\text{sh}}/10^4 \text{ km s}^{-1})$ . The dotted line shows a more average trend:  $\alpha = 0.7 + 0.3 \log_{10}(v_{\text{sh}}/10^4 \text{ km s}^{-1})$ .

## 8 REFERENCES

- Achterberg A., Gallant Y.A. Kirk J.G. & Guthmann A.W., 2001, MNRAS 328, 393  
 Allen G. E., Houck J. C. & Sturmer S. J., 2008, ApJ, 683, 773  
 Axford W.I., Leer E., Skadron G., 1977, Proc 15th Int. Cosmic Ray Conf., 11, 132  
 Baars J. W. M., Genzel R., Pauliny-Toth I. I. K. & Witzel A., 1977, A & A, 61, 99  
 Baring M.G., Ellison D.C. & Jones F.C., 1993, ApJ, 409, 327  
 Bell A.R., 1978, MNRAS, 182, 147  
 Bell A.R. 1987 MNRAS, 225, 615  
 Bell A.R., 2004, MNRAS, 353, 550  
 Bell A.R., 2005, MNRAS, 358, 181  
 Bell A.R., Robinson A.P.L., Sherlock M. Kingham R.J. & Rozmus W., 2006, Plasma Phys Cont Fusion, 48, R37  
 Blandford R.D. & Ostriker J.P., 1978, ApJ, 221, L29  
 Bocchino F., Orlando S., Miceli M. & Petruk O., 2011, A&A 539, 129  
 Chen Y., Su Y., Slane P. O. & Wang Q. D., 2004, ApJ, 616, 885  
 Chevalier R. A., 1998, ApJ, 499, 810  
 Chevalier R. A. & Fransson C., 2006, ApJ, 651, 381  
 Chiotellis A., Schure K. M., & Vink J., 2011 arXiv 1103.5487  
 Crawford F., Gaensler B. M., Kaspi V. M., Manchester R. N., Camilo F., Lyne A. G. & Pivovarov M. J. 2001, ApJ, 554, 152  
 Drury L.O'C., 1983, Rep Prog Phys, 46, 973  
 Drury L.O'C. & Völk H.J., 1981, ApJ 248, 344  
 Ellison D.C., Baring M.G & Jones F.C., 1996, ApJ 473, 1029  
 Ellison D. C. & Reynolds S. P., 1991, ApJ, 382, 242  
 Falle S.A.E.G. & Giddings J.R. 1987 MNRAS 225, 399  
 Gaensler B. M., Manchester R. N. & Green A. J., 1998, MNRAS, 296, 813  
 Gaisser TK, Protheroe RJ & Stanev T, 1998, ApJ 492, 219  
 Giacalone, J. & Jokipii, J.R., 2007, ApJ 663, L41  
 Gieseler U.D.J., Kirk J.G., Gallant Y.A. & Achterberg A.,

1999, A&A 345 298  
 Glushak A.P., 1985, Pis'ma Astron Zh 11, 825  
 Gómez Y., & Rodríguez L. F. 2009 Rev Mex Astron Astrophys 45, 91  
 Gotthelf E. V., Petre R. & Hwang U., 1997, ApJL, 487, L175  
 Green D. A., 2009, <http://www.mrao.cam.ac.uk/surveys/snrs/>  
 Greiner J., Egger R. & Aschenbach B., 1994, A & A, 286, L35  
 Harrus I. M. & Slane P. O., 1999, ApJ, 516, 811  
 Haslam C. G. T., Salter C. J. & Pauls T., 1980, A & A, 92, 57  
 Helder E. A., Vink J., Bassa C. G., Bamba A., Bleeker J. A. M., Funk S., Ghavamian P., van der Heyden K. J., Verbunt F. & Yamazaki R., 2009, Science 325, 719  
 Hillas A.M., 2005, J Phys G 31, R95  
 Huba J.D., 1994, NRL Plasma Formulary, publ. Naval Research Laboratory, Washington, USA  
 Hwang U., Petre R. & Hughes J. P., 2000, ApJ, 532, 970  
 Johnston T.W., 1960, Phys Rev 120, 1103  
 Jokipii J.R., 1982, ApJ 215, 716  
 Jokipii J.R., 1987, ApJ 313, 842  
 Katz-Stone D. M., Kassim N. E. Lazio T. J. W. & O'Donnell R., 2000, ApJ, 529, 453  
 Kinugasa K. Torii K. Tsunemi H., Yamauchi S., Koyama K. & Dotani T., 1998, Publ. Astron. Soc. Japan, 50, 249  
 Kirk J.G., Duffy P. & Gallant Y.A., 1996, A&A 314, 1010  
 Kirk J.G. & Heavens A.F., 1989, MNRAS 239, 995  
 Kobayakawa K., Honda Y.S. & Samura T., 2002, Phys Rev D 66 083004  
 Krymskii G.F., 1977, Sov Phys Dokl, 23, 327  
 Manchester R. N., Gaensler B. M., Staveley-Smith L., Kesteven M. J. & Tzioumis A. K., 2005, ApJL, 628, L131  
 Manchester R. N., Gaensler B. M., Wheaton V. C., Staveley-Smith L., Tzioumis A. K., Bizunok N. S., Kesteven M. J. & Reynolds J. E., 2002, Pub. Astr. Soc. Austr., 19, 207  
 Ostrowski M., 1991, MNRAS 249 551  
 Ostrowski M., 1999, A&A, 345, 256  
 O'Sullivan C. & Green D. A., 1999, MNRAS, 303, 575  
 Rakowski C. E., Hughes J. P. & Slane, P., 2001, ApJ, 548, 258  
 Rothenflug R., Balle, J., Dubner G., Giacani E., Decourchelle A. & Ferrando, P., 2004, A&A, 425, 121  
 Ruffalo D., 1999, ApJ 515 787  
 Sankrit R., Blair W. P., Delaney T., Rudnick L., Harrus I. M. & Ennis J. A., 2005, Advances in Space Research, 35, 1027  
 Schure K. M., Achterberg A., Keppens R. & Vink J., 2010, MNRAS 406, 2633  
 Slane P., Chen Y., Lazendic J. S. & Hughes J. P., 2002, ApJ, 580, 904  
 Tian W. W., Leahy D. A., 2008, MNRAS, 391, L54  
 Weiler K. W., Williams C. L., Panagia N., Stockdale C. J., Kelley M. T., Sramek R. A., Van Dyk S. D. & Marcaide J. M., 2007, ApJ, 671, 1959  
 Wright M., Dickel J., Koralesky B. & Rudnick L., 1999, ApJ, 518, 284  
 Zhou X., Chen Y., Su Y. & Yang J., 2009, ApJ, 691, 516  
 Zirakashvili V.N. & Ptuskin V.S., 2008, ApJ 678, 939

| SNR                   | diameter<br>pc   | age<br>years      | velocity (R/t)<br>$10^3 \text{ km s}^{-1}$ | $\alpha$ |
|-----------------------|------------------|-------------------|--|----------|
| G1.9+0.3              | 3.7              | 220 <sup>b</sup>  | 9  | 0.6      |
| G4.5+6.8 (Kepler)     | 6 <sup>c</sup>   | 400               | 7.3  | 0.64     |
| G11.2-0.3 (SN 386)    | 5.1              | 1620              | 1.5  | 0.6      |
| G21.8-0.6 (Kes 69)    | 32               | 4600 <sup>d</sup> | 3.4  | 0.5      |
| G27.4+0.0 (Kes 73)    | 10               | 1000 <sup>e</sup> | 4.9  | 0.68     |
| G29.7-0.3 (Kes 75)    | 6.6              | 884               | 3.7  | 0.7      |
| G31.9+0.0 (3C391)     | 14.8             | 4000 <sup>f</sup> | 1.8  | 0.49     |
| G39.2-0.3 (3C396)     | 15.5             | 7100 <sup>g</sup> | 1.1  | 0.6      |
| G43.3-0.2 (W49B)      | 11.6             | 4000 <sup>h</sup> | 1.4  | 0.48     |
| G93.3+6.9 (DA 530)    | 16               | 3000 <sup>i</sup> | 2.6  | 0.45     |
| G111.7-2.1 (Cas A)    | 5                | 330               | 7.4  | 0.77     |
| G120.1+1.4 (Tycho)    | 6                | 440               | 6.7  | 0.65     |
| G272.2-3.2            | 7.9 <sup>j</sup> | 1100              | 3.5  | 0.6      |
| G292.2-0.5            | 44               | 1700 <sup>k</sup> | 13   | 0.5      |
| G296.8-0.3            | 56               | 6000 <sup>l</sup> | 4.6  | 0.6      |
| G315.4-2.3 (RCW86)    | 28               | 1825              | 7.5  | 0.6      |
| G327.6+14.6 (SN1006)  | 19.2             | 1000              | 9.4  | 0.6      |
| G332.4-0.4 (RCW103)   | 9                | 4000 <sup>m</sup> | 4.4  | 0.5      |
| G337.2-0.7            | 10               | 3000 <sup>n</sup> | 1.6  | 0.4      |
| G349.7+0.2            | 16               | 2800 <sup>p</sup> | 2.8  | 0.5      |
| G352.7-0.1            | 17               | 2200 <sup>q</sup> | 3.1  | 0.6      |
| SN1987A <sup>r</sup>  | 0.34             | 6                 | 35   | 0.9      |
| SN1987A <sup>s</sup>  | 0.41             | 16                | 10   | 0.8      |
| SN1993J <sup>t</sup>  | 0.24             | 10                | 15   | 0.81     |
| SN1983N <sup>v</sup>  |                  |                   | 42   | 1.0      |
| SN1984L <sup>v</sup>  |                  |                   | 100  | 1.0      |
| SN1990B <sup>v</sup>  |                  |                   | 33   | 1.0      |
| SN1994I <sup>v</sup>  |                  |                   | 38   | 1.0      |
| SN2001ig <sup>v</sup> |                  |                   | 49   | 1.06     |
| SN2002ap <sup>v</sup> |                  |                   | 105  | 0.9      |
| SN2003L <sup>v</sup>  |                  |                   | 32   | 1.1      |
| SN2003bg <sup>v</sup> |                  |                   | 44   | 1.1      |
| SN1998bw <sup>v</sup> |                  |                   | 60   | 0.75     |

**Table 1.** Overview of the supernova remnant models. Data are taken from the updated Galactic SNR catalogue by Green (2009) unless other source specified. Other sources: <sup>b</sup>Gomez & Rodriguez (2009), <sup>c</sup>Sankrit et al (2005), Chiotellis et al (2011), <sup>d</sup>Zhou et al (2009), <sup>e</sup>Tian & Leahy (2008), <sup>f</sup>Chen et al (2004), <sup>g</sup>Harrus & Slane (1999), <sup>h</sup>Hwang et al (2000), <sup>i</sup>Haslam et al (1980), <sup>j</sup>Greiner et al (1994), <sup>k</sup>Crawford et al (2001), <sup>l</sup>Gaensler et al (1998), <sup>m</sup>Gotthelf et al (1997), <sup>n</sup>Rakowski et al (2001), <sup>p</sup>Slane et al, <sup>q</sup>Kinugasa et al (1998), <sup>r</sup>Manchester et al (2002), <sup>s</sup>Manchester et al (2005), <sup>t</sup>Weiler et al (2007), <sup>v</sup>Chevalier & Fransson (2006)